




Investigation of the one-neutron transfer in $^{13}\text{C} + ^{28}\text{Si}$ at $E_{\text{lab}} = 30$ and 34 MeVR. Linares ^{1,*}, C. C. Seabra,¹ V. A. B. Zagatto,¹ V. Scarduelli,^{1,2} L. Gasques,² L. C. Chamon ², B. R. Gonçalves,¹ D. R. Mendes Junior,¹ and A. Lépine-Szily ²¹Instituto de Física, Universidade Federal Fluminense, 24210-340, Niterói, Rio de Janeiro, Brazil²Instituto de Física, Universidade de São Paulo, São Paulo, Brazil

(Received 24 October 2019; published 21 January 2020)

Background: Neutron transfer measurements for the $^{18}\text{O} + ^{28}\text{Si}$ system have shown that the experimental one-neutron and two-neutron transfer cross sections are well reproduced with spectroscopic amplitudes from two different shell-model interactions for the Si isotopes: *psdmod* for the two-neutron transfer, and *psdmwkp* for the one-neutron transfer.

Purpose: The need for two distinct shell-model interactions to reproduce two neutron-transfer processes in the same nuclei may cover a more complex mechanism in the one-neutron transfer that requires the unpairing of neutrons prior to its transfer in the (^{18}O , ^{17}O) reaction. Studying a nucleus where this characteristic is absent (^{13}C) should help to elucidate this question.

Method: One-neutron transfer cross sections were measured for the $^{13}\text{C} + ^{28}\text{Si}$ at $E_{\text{lab}} = 30$ and 34 MeV, and compared with coupled reaction channel calculations using spectroscopic amplitudes derived from the *psdmod* and *psdmwkp* shell-model interactions.

Results: The spectroscopic amplitudes from the *psdmod* interaction for the relevant states in ^{29}Si provide a good description of the experimental data and the corresponding values agree with previous estimates obtained from the (d , p) reaction.

Conclusions: The experimental data for the one-neutron transfer to ^{28}Si induced by (^{13}C , ^{12}C) reaction is well reproduced using spectroscopic amplitudes from the *psdmod*.

DOI: [10.1103/PhysRevC.101.014611](https://doi.org/10.1103/PhysRevC.101.014611)

I. INTRODUCTION

Particle configurations of bound states in the atomic nuclei can be studied using transfer reactions. In such studies, the optical potential and spectroscopic factors (S^2) are important parameters in the calculations of the transfer cross sections. Experimental values for S^2 can be obtained from a direct comparison between experimental and theoretical cross sections, as in (d , p) [1,2], (t , d) [3], and (^7Li , ^6Li) [4] reactions. However, the experimental approach may lead to some ambiguities in the S^2 values for many nuclei. For instance, the S^2 value for a $p_{1/2}$ valence neutron to ^{12}C ranges from 0.3 [from $^{13}\text{C}(p, d)^{12}\text{C}$ data at 65 MeV [5]] to 1.4 [from $^{12}\text{C}(d, p)^{13}\text{C}$ data at 15 MeV [6]]. The main reasons for these discrepancies are the adopted optical potentials and the coupling scheme considered in direct reaction calculations [7].

Recent advances in experimental setups have renewed the use of heavy-ion probes, like (^{13}C , ^{12}C) and (^{18}O , ^{17}O), in transfer reactions [8]. Some advantages over the use of light ions are (i) avoidance of the inclusion of the break-up channel [9], and (ii) suppression of the effect of nonlocality, which is relevant in (d , p) reactions [10,11]. On the other hand, effects of strong absorption are more pronounced and the angular distributions exhibit a diffraction-like pattern as

the bombarding energy increases. Moreover, second-order mechanisms such as projectile or target excitation preceding and/or following the transfer of nucleons must be taken into account properly. In addition, partial waves that contribute to the transfer reaction are limited to a range of optimum Q values for a given reaction and energy.

Recently, analysis of the one-neutron transfer (1NT) and two-neutron transfer (2NT) to ^{28}Si , induced by the (^{18}O , ^{17}O) [12] and (^{18}O , ^{16}O) [13] reactions, respectively, have been reported. In these works, coupled reaction channels (CRCs) were performed including S^2 for the relevant states derived from nuclear shell models with suitable interactions and model spaces to describe the low-lying states in the $^{28,29,30}\text{Si}$ isotopes. Best agreement between experimental data and calculations have been achieved adopting different interactions for the 1NT (*psdmwkp*) and 2NT (*psdmod*) processes.

It is not clear how the 1NT is affected by the preformed paired valence neutrons in the ^{18}O nucleus. In this work, we analyzed the 1NT to ^{28}Si by using a (^{13}C , ^{12}C) probe. ^{13}C is treated as a single valence neutron bound to a ^{12}C nuclear core. We measured elastic cross sections at $E_{\text{lab}} = 25$, 30, and 34 MeV and inelastic and one-neutron transfer cross sections at $E_{\text{lab}} = 30$ and 34 MeV. Cross sections for elastic and inelastic scattering are used to constrain the parameters of the effective nucleus-nucleus potential.

This paper is organized as follows: the experimental details and the theoretical analysis are discussed in Secs. II and III, respectively. The conclusions are given in Sec. IV.

*rlinares@id.uff.br

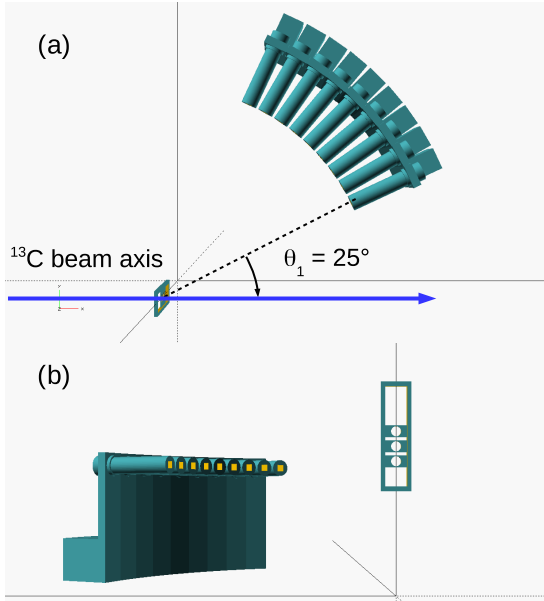


FIG. 1. Sketch of the experimental setup with an array of 9 Si detectors mounted in angular steps of 5° with the first one at $\theta_{\text{lab}} = 25^\circ$. Panel (a) shows a top view of the setup and panel (b) shows a frontal view.

II. EXPERIMENTAL DETAILS

The experiment was performed at the 8 MV tandem accelerator of the University of São Paulo. The ^{13}C beam was accelerated at $E_{\text{lab}} = 25, 30,$ and 34 MeV with averaged beam intensity of about 30 enA on the target. For the $^{13}\text{C} + ^{28}\text{Si}$ system, the Coulomb barrier height is $V_B = 18.9$ MeV (in the laboratory reference frame).

Figure 1 shows a sketch of the Silicon Array and Telescopes of Usp for Reactions and Nuclear applications (SATURN) system [14], mounted in the scattering chamber for the measurements. A set of nine surface barrier Si detectors was mounted 30 cm away from the targets and with 5° of angular step size, covering the angles from 25° to 65° (laboratory framework). A four-position mobile target ladder, placed at the center of the chamber, was mounted with two thin ^{28}Si foils (Si-only) 99.9% isotopically enriched and two other foils composed of ^{28}Si with a thin backing layer of ^{197}Au (Si + Au). Thicknesses of the ^{28}Si layers were measured by Rutherford backscattering (RBS) of ^4He beam and were approximately $40 \mu\text{g}/\text{cm}^2$.

At each beam energy, measurements were carried out with the Si + Au target, for normalization of the cross sections, and the Si-only target, for a clear identification of the INT. The energy calibration of each Si detector was performed by adopting the elastic peaks associated with the ^{13}C scattered off the ^{28}Si and ^{197}Au nuclei. The energy resolution achieved was 0.2 MeV. The ratio between Au and Si foil thicknesses was determined from measurements at $E_{\text{lab}} = 25$ MeV, using the angular points at $\theta_{\text{lab}} = 25^\circ, 30^\circ,$ and 35° , and the theoretical curve.

Typical Q -energy spectra, defined as the energy relative to the elastic scattering in the $^{13}\text{C} + ^{28}\text{Si}$, are shown in Figs. 2(a)

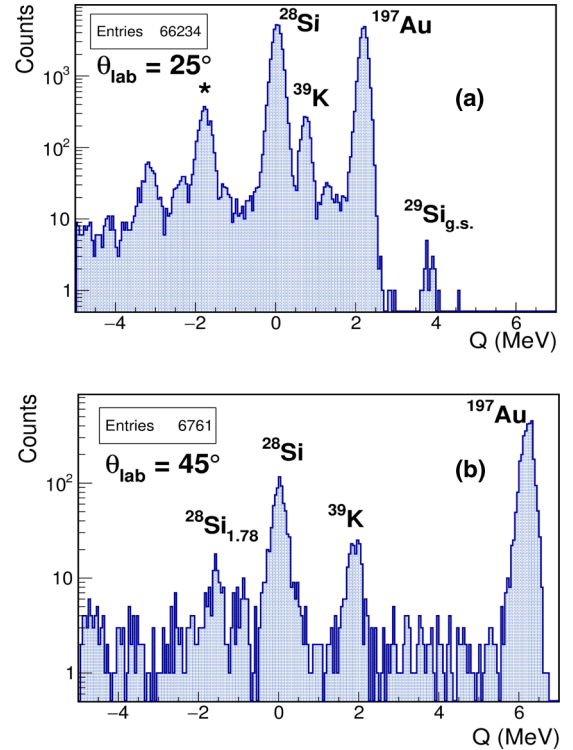


FIG. 2. The Q -energy spectrum for the measurements with ^{13}C at 34 MeV on the Si + Au target. The spectra observed at $\theta_{\text{lab}} = 25^\circ$ and 45° are shown in panels (a) and (b), respectively. The asterisk in panel (a) indicates the presence of oxygen contamination (in the target) in the inelastic peak.

and 2(b) at $\theta_{\text{lab}} = 25^\circ$ and 45° , respectively, measured at $E_{\text{lab}} = 34$ MeV. In this representation, the elastic scattering from ^{28}Si corresponds to a peak centered at $Q = 0.0$ MeV. The inelastic peak associated with the excitation of $^{28}\text{Si}_{1.78}$ MeV corresponds to the peak around $Q = -1.8$ MeV. At forwards angles, scattering off contaminants (oxygen) present in the target superimposes with the inelastic peak, as indicated by the asterisk in Fig. 2(a). Scattering off the ^{197}Au corresponds to peaks with $Q > 0$ with Q energy that depends on the scattering angle.

For the $^{13}\text{C} + ^{28}\text{Si}$ system, the Q -value for 1NT ground state \rightarrow ground state (g.s.) is $+3.53$ MeV and, therefore, this reaction channel is energetically distinguished from elastic and inelastic events. In Fig. 2(a), the peak at $Q = +3.6$ MeV ($^{29}\text{Si}_{\text{g.s.}}$) is associated with the 1NT g.s. \rightarrow g.s. At $\theta_{\text{lab}} = 45^\circ$, the inelastic excitations of the ^{197}Au interfere with the $^{29}\text{Si}_{\text{g.s.}}$ peak [see Fig. 2(b)]. Between the elastic of ^{28}Si and ^{197}Au it is also observed a peak that comes from ^{39}K contamination in the target carried in during the manufacturing process of the thin films. The presence of this contamination was also confirmed with the Rutherford backscattering spectrometry (RBS) analysis of the foils produced in the same batch, indicating a 2% K contamination in the target.

A typical spectrum for a Si-only target is shown in Fig. 3 (blue histogram). The 1NT to the $^{29}\text{Si}_{\text{g.s.}}$, the elastic peak of the ^{28}Si , and inelastic peak of the $^{28}\text{Si}_{1.78}$ correspond to peaks 1, 4, and 6, respectively. Other peaks associated with

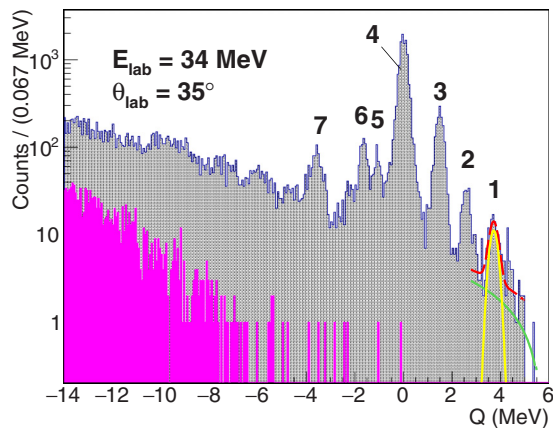


FIG. 3. The Q -energy spectrum for the measurements with ^{13}C at 34 MeV on the Si-only target at $\theta_{\text{lab}} = 35^\circ$ (blue histogram). In the same plot is shown the energy spectrum of p and α from a fusion-evaporation process (purple histogram). Peak numbering is as follows: 1: $^{29}\text{Si}_{\text{g.s.}}$ (1NT); 2: $^{29}\text{Si}_{1,27}$ and $^{40}\text{K}_{\text{g.s.}}$ (1NT); 3: elastic peak ^{39}K ; 4: elastic peak ^{28}Si ; 5: possibly inelastic peak in $^{39}\text{K}_{2,52}$; 6: inelastic peak $^{28}\text{Si}_{1,78}$; 7: elastic peak ^{16}O and ^{12}C . Counts in peak 1 were determined from the Gaussian curve represented by the yellow curve. See text for further details.

reactions with contaminants on the target were also identified (listed in the caption of Fig. 3), except peak 5. This is possibly associated with the inelastic scattering that populates the $1/2^+$ (2.52 MeV) in ^{39}K . Calculation of the energies of p and α particles coming from the fusion-evaporation process, using the PACE4 code [15,16], is presented in Fig. 3 (purple histogram). This shows that, in the energy range of the $^{29}\text{Si}_{\text{g.s.}}$ peak, there is no significant interference of highly energetic p or α particles.

Yields in the elastic, inelastic, and 1NT were determined from a Gaussian curve on top of a linear background fit to the experimental peaks. An example of such fits is shown in Fig. 3 in which the Gaussian (yellow curve) and the linear (green curve) components are reproduced for the peak number 1. There are some counts with Q value higher than +4.0 MeV that may come from contaminant heavier than K in the Si-only target. Possible heavy contaminants are ^{127}I , from the release agent, and ^{184}W , from the cathode used as holder for the ^{28}Si powder for the manufacturing of the thin films. Such heavier contaminants were not observed in the RBS analysis. Even though, in both cases, the elastic scattering of ^{13}C would produce peaks at Q values of +4.1 and +4.5 MeV, respectively. For the inelastic peak, the background due to the presence of peak 5 at some angles was subtracted adopting a linear behavior.

III. THEORETICAL ANALYSIS

Direct reaction calculations were performed within the coupled reaction channel (CRC) framework using the FRESKO code [17] with exact finite range and prior representation. Nonorthogonality corrections and full complex remnant terms were considered in the coupled-channel equations. A sketch of the coupling scheme considered in the CRC calculations

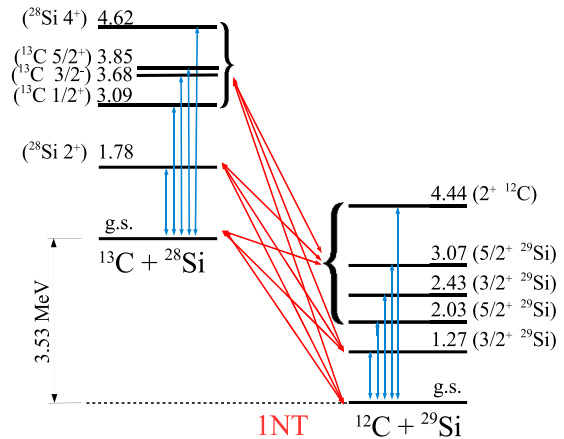


FIG. 4. Coupling scheme considered in the CRC calculations.

is shown in Fig. 4. The inelastic channels were considered by using the deformation parameter for the collective states. For the ^{28}Si target nucleus, $\beta_2 = 0.407$, taken from Ref. [18], and for the ^{13}C projectile nucleus, $\beta_1 = 0.143$ [19]. The single-particle wave functions used in the matrix elements were generated by using Woods-Saxon potential with depth adjusted to reproduce the experimental separation energies for one neutron in ^{13}C ($S_n = 4.95$ MeV) and ^{29}Si ($S_n = 8.45$ MeV). The reduced radii and diffuseness parameters for the ^{28}Si and ^{12}C cores were set to values previously used in the analysis with the ^{18}O projectile. These values are 1.26 and 0.65 fm for the ^{28}Si core [13] and 1.25 and 0.80 fm for ^{12}C [20], respectively. Calculations have been performed within 10% deviation in the adopted reduced radii and diffuseness values and no significant effect were observed in the results.

The S^2 values were obtained by using the NUSHELLX code [21]. For $^{12,13}\text{C}$, the calculations were performed by using the *psdmod* interaction, which is a modified version of the *psdwb* interaction [22], which gives a reasonable description of the p - sd -shell nuclei. For $^{28,29}\text{Si}$ isotopes, two interactions are considered: again the *psdmod* and the *psdmwkp* interactions [23]. The latter is a combination of the Cohen-Kurath interaction [24] for the p shell, the Wildenthal interaction [25] for the sd -shell, and the Millener-Kurath interaction [26] for the coupling matrix elements between p and sd shells. In both interactions, the model space assumes ^4He as a closed core and valence neutrons and protons in the $1p_{3/2}$, $1p_{1/2}$, $1d_{5/2}$, $1d_{3/2}$, and $2s_{1/2}$ orbitals. The spectroscopic amplitudes of states in ^{29}Si for both interactions can be found in Ref. [12]. For clarity, from now on CRC-*psdmod* and CRC-*psdmwkp* stand for the CRC calculations using S^2 for ^{29}Si derived from the *psdmod* and *psdmwkp* interactions, respectively.

For the CRC, the São Paulo double folding potential (SPP) [27] was used for the real and imaginary parts of the optical potential. In the entrance partition, N_i was adjusted to describe the experimental data for elastic and inelastic scatterings to account for couplings not explicitly considered in the coupling scheme.

Figure 5 shows the angular distributions of the elastic cross sections for $E_{\text{lab}} = 25, 30,$ and 34 MeV. Optical model calculations using an internal imaginary potential is shown as

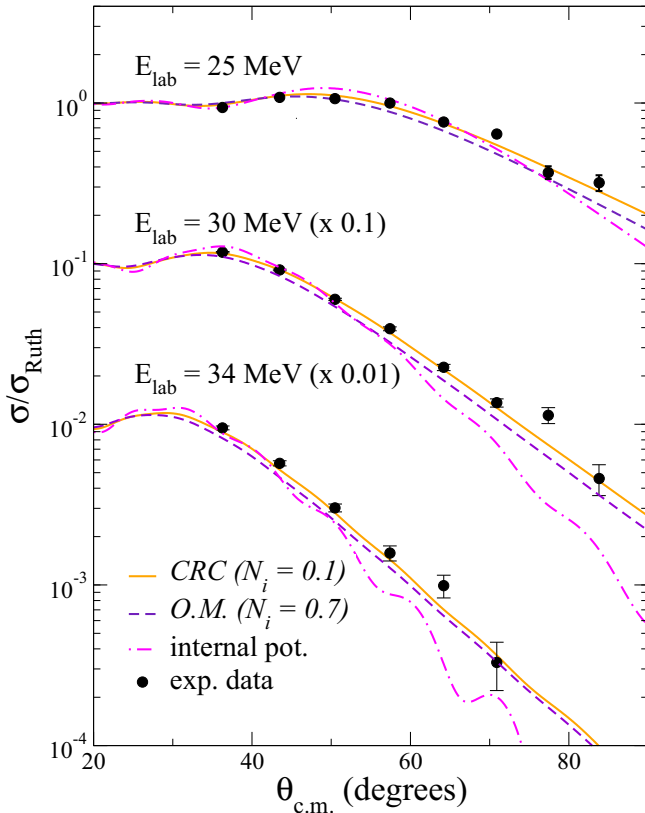


FIG. 5. Angular distributions of the elastic cross sections for the $^{13}\text{C} + ^{28}\text{Si}$ at $E_{\text{lab}} = 25, 30,$ and 34 MeV. The data points at $\theta_{\text{lab}} = 25^\circ, 30^\circ,$ and 35° for $E_{\text{lab}} = 25$ MeV were adopted for normalization of the cross sections.

a dot-dashed purple curve. The internal imaginary potential was defined as a Wood-Saxon shape with depth, reduced radius, and diffuseness set to 50 MeV, 1.06 fm, and 0.2 fm, respectively. This optical potential underestimates the cross sections at large scattering angles. A second optical model calculation was performed by using the SPP shape for the imaginary part with adjustable N_i factor. The best agreement between experimental data and theoretical curves is achieved for $N_i = 0.7$, in Fig. 5 represented as dashed blue curves. In the CRC calculations, experimental data are well reproduced with $N_i = 0.1$ in the entrance optical potential. Similar results are obtained for $N_i = 0.2$ and 0.3 (not shown in Fig. 5). This indicates that most relevant reaction channels (inelastic and INT) are accounted for in the coupling scheme and, consequently, a smaller imaginary factor is required.

The angular distributions of the inelastic cross sections to the 2^+ excited state in ^{28}Si for $E_{\text{lab}} = 30$ and 34 MeV are shown in Fig. 6, along with CRC calculations with different N_i in the imaginary term of the optical potential. Good overall agreements between experimental data and CRC calculations are achieved for $N_i = 0.1$ and 0.2 . The theoretical curves for the elastic scattering with these N_i are almost indistinguishable. The fit to elastic and inelastic data provides a good constrain on the parameter of the imaginary potential.

The cross sections for the INT at $E_{\text{lab}} = 30$ and 34 MeV are shown in Fig. 7. The CRC-*psdmod* and CRC-*psdmwkp*

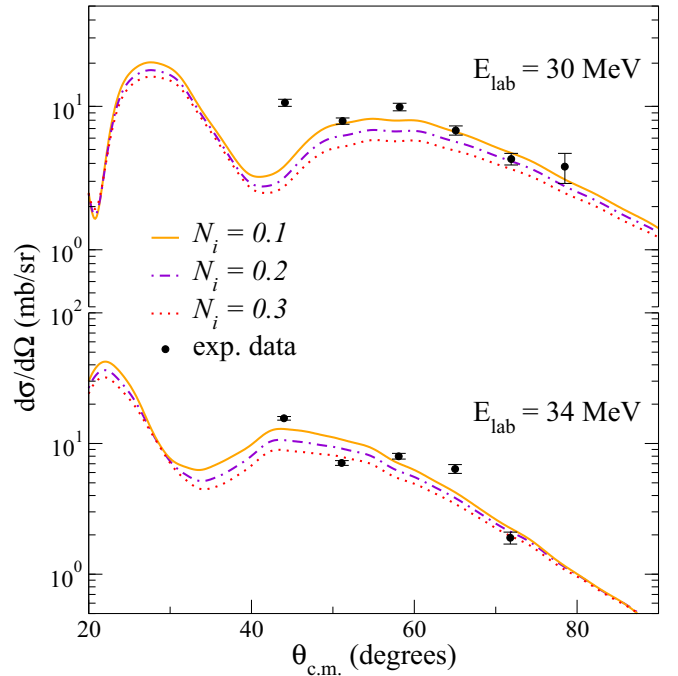


FIG. 6. Angular distributions of the inelastic 2^+ in ^{28}Si cross sections for $^{13}\text{C} + ^{28}\text{Si}$ at $E_{\text{lab}} = 30$ and 34 MeV.

calculations were performed using $N_i = 0.1$ in the optical potential of the entrance partition. Similar results are obtained using $N_i = 0.2$ and 0.3 , meaning that the effect of N_i values, between 0.1 and 0.3 , is not strong on the INT channel. In the exit partition, the imaginary strength factor (N_i) was set to 0.78 , since this value provides a good description of the elastic scattering cross section for many systems in a wide energy interval [28]. The effect of reduced radii and

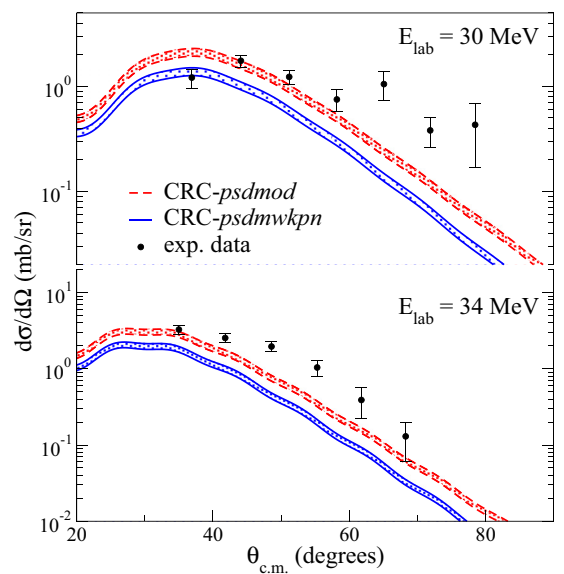


FIG. 7. Angular distributions of the INT leading to the population of the g.s. in ^{29}Si cross sections for $^{13}\text{C} + ^{28}\text{Si}$ at $E_{\text{lab}} = 30$ and 34 MeV.

TABLE I. Spectroscopic factors \mathcal{S}^2 for the ^{28}Si to ^{29}Si transitions obtained by shell-model calculations using *psdmod* and *psdmwkp*n interactions. Values obtained from $^{28}\text{Si}(d, p)^{29}\text{Si}$ of Refs. [1,2,29] are also included.

State		$ \mathcal{S} ^2$				
Initial	Final	<i>psdmod</i>	<i>psdmwkp</i> n	Ref. [1]	Ref. [2]	Ref. [29]
$^{28}\text{Si}_{\text{g.s.}}$	$^{29}\text{Si}_{\text{g.s.}}$	0.51	0.32	0.53	0.37	0.42 ± 0.13

diffuseness parameters, used in the form factor to construct the single-particle wave functions of ^{13}C and ^{29}Si , has been checked. The reduced radii and diffuseness values were varied within the 1.20–1.25 fm and 0.7–0.8 fm ranges, respectively. These are represented in the envelope curves for each CRC calculation in Fig. 7. The theoretical curves are more sensitive to the diffuseness parameter. However, the overall effect in the calculations is not so crucial and the CRC-*psdmwkp*n curves systematically lie below the CRC-*psdmod*. The coupling space has also been checked and the results for elastic, inelastic, and INT are practically the same with the removal of $3/2^-$ and $5/2^+$ states in ^{13}C and the 4^+ state in ^{28}Si .

CRC-*psdmod* reproduces better the experimental values at $E_{\text{lab}} = 34$ MeV and the agreement is limited at 30 MeV. Nevertheless, the CRC-*psdmwkp*n underestimates the cross sections at both energies. This indicates that the *psdmod* interaction provides a better estimate for the \mathcal{S}^2 of the $^{28,29}\text{Si}$ isotopes. Table I presents a comparison between the spectroscopic factors (\mathcal{S}^2) for the ^{28}Si to ^{29}Si transitions derived from the *psdmod* and *psdmwkp*n interactions and experimental estimates obtained from the (d, p) reaction and distorted wave Born approximation calculations [1,2,29]. The value of \mathcal{S}^2 from *psdmod* is close to the one reported in Ref. [1] whereas the *psdmwkp*n estimate is closer to that in Ref. [2]. All values are within the one-uncertainty interval obtained from a systematic analysis of experimental data for (d, p) and using a deuteron optical potential which approximately accounts for deuteron breakup [29].

The success of CRC-*psdmod* compared with the present data is consistent with analysis of 2NT in $^{28}\text{Si}(^{18}\text{O}, ^{16}\text{O})^{30}\text{Si}$, for which the experimental data were reproduced adopting the \mathcal{S}^2 derived from the *psdmod* interaction for the Si isotopes [13]. In the analysis of INT to ^{28}Si induced by the $(^{18}\text{O}, ^{17}\text{O})$ reaction, the experimental data were reproduced better by using \mathcal{S}^2 from the *psdmwkp*n interaction [12] instead. The fact that different shell-model interactions are adopted for the description of the INT and 2NT experimental data are interpreted as follows: Accurate prediction for transfer reac-

tion demands a proper description of the nuclear structure of the nuclear partners, represented by \mathcal{S}^2 , reliable optical potential for the scattering and also a detailed description of the transfer process. The usual picture of the ^{18}O nuclei is a dineutron valence particle bound to a ^{16}O core. Therefore, the INT induced by ^{18}O occurs first by breaking the short-range pairing interaction of the two neutrons and, then, one neutron is transferred to the target nuclei. Such dynamics of pairing between two neutrons is not considered in detail in the CRC framework. The use of the *psdmwkp*n interaction for the $(^{18}\text{O}, ^{17}\text{O})$ reaction may have covered up what is, in fact, an effect of the transfer mechanism instead of the nuclear structure of ^{29}Si .

IV. CONCLUSIONS

The INT cross sections in the $^{28}\text{Si}(^{13}\text{C}, ^{12}\text{C})^{29}\text{Si}$ reaction were measured at $E_{\text{lab}} = 30$ and 34 MeV. Within the CRC framework, the optical potential was adjusted to describe experimental data for elastic scattering at $E_{\text{lab}} = 25, 30,$ and 34 MeV and the inelastic scattering at $E_{\text{lab}} = 30$ and 34 MeV. The CRC calculation revealed the necessity to include a small imaginary term on the optical potential to account for reaction channels not explicitly included in the coupling scheme. This was performed by using the São Paulo potential with imaginary normalization of $N_i = 0.1$ and indicates that some given channel has not been explicitly coupled to calculations. Elastic, inelastic, and transfer data have been properly described by using such a configuration. The spectroscopic amplitudes obtained from the *psdmod* shell-model interaction provides a good description of the experimental data and is in accordance with previous analysis of the (d, p) data.

ACKNOWLEDGMENTS

This project has received funding from Conselho Nacional de Desenvolvimento Científico e Tecnológico (CNPq), Fundação de Amparo à Pesquisa do Estado do Rio de Janeiro (FAPERJ), Fundação de Amparo à Pesquisa do Estado de São Paulo (FAPESP), and Coordenação de Aperfeiçoamento de Pessoal de Nível Superior (CAPES) and from Instituto Nacional de Ciência e Tecnologia – Física Nuclear e Aplicações (INCT-FNA). We would also like to thank the technical staff of LAFN for assisting in the maintenance and operation of the accelerator. This research has also used resources of the Laboratory of Material Analysis with Ion Beams - LAMFI-USP. The authors acknowledge the laboratory staff for assistance during the RBS experiments.

- [1] M. C. Mermaz, C. A. Whitten, J. W. Champlin, A. J. Howard, and D. A. Bromley, *Phys. Rev. C* **4**, 1778 (1971).
 [2] R. Peterson, C. Fields, R. Raymond, J. Thieke, and J. Ullman, *Nucl. Phys. A* **408**, 221 (1983).
 [3] K. Pearce, N. Clarke, R. Griffiths, P. Simmonds, D. Barker, J. England, M. Mannion, and C. Ogilvie, *Nucl. Phys. A* **467**, 215 (1987).

- [4] P. Schumacher, N. Ueta, H. Duhm, K.-I. Kubo, and W. Klages, *Nucl. Phys. A* **212**, 573 (1973).
 [5] K. Hosono, M. Kondo, T. Saito, N. Matsuoka, S. Nagamachi, T. Noro, H. Shimizu, S. Kato, K. Okada, K. Ogino, and Y. Kadota, *Nucl. Phys. A* **343**, 234 (1980).
 [6] S. Darden, S. Sen, H. Hiddleston, J. Aymar, and W. Yoh, *Nucl. Phys. A* **208**, 77 (1973).

- [7] X. D. Liu, M. A. Famiano, W. G. Lynch, M. B. Tsang, and J. A. Tostevin, *Phys. Rev. C* **69**, 064313 (2004).
- [8] F. Cappuzzello, C. Agodi, M. Cavallaro, D. Carbone, S. Tudisco, D. Lo Presti, J. R. B. Oliveira, P. Finocchiaro, M. Colonna, D. Rifuggiato, L. Calabretta, D. Calvo, L. Pandola, L. Acosta, N. Auerbach, J. Bellone, R. Bijker, D. Bonanno, D. Bongiovanni, T. Borello-Lewin *et al.*, *Eur. Phys. J. A* **54**, 72 (2018).
- [9] G. W. Bailey, N. K. Timofeyuk, and J. A. Tostevin, *Phys. Rev. Lett.* **117**, 162502 (2016).
- [10] N. K. Timofeyuk and R. C. Johnson, *Phys. Rev. Lett.* **110**, 112501 (2013).
- [11] A. Ross, L. J. Titus, and F. M. Nunes, *Phys. Rev. C* **94**, 014607 (2016).
- [12] R. Linares, M. J. Ermamatov, J. Lubian, F. Cappuzzello, D. Carbone, E. N. Cardozo, M. Cavallaro, J. L. Ferreira, A. Foti, A. Gargano, B. Paes, G. Santagati, and V. A. B. Zagatto, *Phys. Rev. C* **98**, 054615 (2018).
- [13] E. N. Cardozo, J. Lubian, R. Linares, F. Cappuzzello, D. Carbone, M. Cavallaro, J. L. Ferreira, A. Gargano, B. Paes, and G. Santagati, *Phys. Rev. C* **97**, 064611 (2018).
- [14] L. R. Gasques, A. S. Freitas, L. C. Chamon, J. R. B. Oliveira, N. H. Medina, V. Scarduelli, E. S. Rossi, M. A. G. Alvarez, V. A. B. Zagatto, J. Lubian, G. P. A. Nobre, I. Padron, and B. V. Carlson, *Phys. Rev. C* **97**, 034629 (2018).
- [15] O. Tarasov and D. Bazin, *Nucl. Instrum. Methods Phys. Res., Sect. B* **266**, 4657 (2008).
- [16] A. Gavron, *Phys. Rev. C* **21**, 230 (1980).
- [17] I. J. Thompson, *Comput. Phys. Rep.* **7**, 167 (1988).
- [18] S. Raman, C. Nestor, Jr., and P. Tikkanen, *At. Data Nucl. Data Tables* **78**, 1 (2001).
- [19] F. Ajzenberg-Selove, *Nucl. Phys. A* **523**, 1 (1991).
- [20] M. Cavallaro, F. Cappuzzello, M. Bondi, D. Carbone, V. N. Garcia, A. Gargano, S. M. Lenzi, J. Lubian, C. Agodi, F. Azaiez, M. De Napoli, A. Foti, S. Franchoo, R. Linares, D. Nicolosi, M. Niikura, J. A. Scarpaci, and S. Tropea, *Phys. Rev. C* **88**, 054601 (2013).
- [21] W. D. M. Rae, <http://www.garsington.eclipse.co.uk> (2008).
- [22] Y. Utsuno and S. Chiba, *Phys. Rev. C* **83**, 021301(R) (2011).
- [23] A. H. Taqi Al-Bayati and S. S. Darwesh, *AIP Conf. Proc.* **1569**, 27 (2013).
- [24] S. Cohen and D. Kurath, *Nucl. Phys.* **73**, 1 (1965).
- [25] B. Wildenthal, *Prog. Part. Nucl. Phys.* **11**, 5 (1984).
- [26] D. Millener and D. Kurath, *Nucl. Phys. A* **255**, 315 (1975).
- [27] L. C. Chamon, B. V. Carlson, L. R. Gasques, D. Pereira, C. De Conti, M. A. G. Alvarez, M. S. Hussein, M. A. Cândido Ribeiro, E. S. Rossi Jr., and C. P. Silva, *Phys. Rev. C* **66**, 014610 (2002).
- [28] M. A. G. Alvarez, L. C. Chamon, M. S. Hussein, D. Pereira, L. R. Gasques, E. S. Rossi, and C. P. Silva, *Nucl. Phys. A* **723**, 93 (2003).
- [29] M. B. Tsang, J. Lee, and W. G. Lynch, *Phys. Rev. Lett.* **95**, 222501 (2005).